

A 3D STOCHASTIC CLOUD MODEL FOR INVESTIGATING THE RADIATIVE PROPERTIES OF INHOMOGENEOUS CIRRUS CLOUDS

Robin J. Hogan* and Sarah F. Kew†

Department of Meteorology, University of Reading, Reading, Berkshire, United Kingdom

1 INTRODUCTION

The importance of ice clouds on the earth's radiation budget is well recognized (Liou 1986), and studies have shown that ice cloud inhomogeneity can have a strong effect on mean fluxes in both the shortwave (Carlin et al. 2002) and longwave (Pomroy and Illingworth 2000). Stochastic models capable of simulating realistic cloud structures are very useful for quantifying this effect, and several such models exist for boundary layer clouds, such as those of Cahalan et al. (1994) and DiGuiseppe and Tompkins (2003) for stratocumulus, and Evans and Wiscombe (2004) for cumulus. In this paper we present the first stochastic model capable of representing the important structural properties unique to cirrus: fallstreak geometry and shear-induced mixing. The model essentially takes 1D power spectra of ice water content obtained from cloud radar, and performs a 3D inverse Fourier Transform with random phases for the Fourier components to obtain an isotropic 3D fractal field with the same spectral properties as the original data. Each vertical layer of the field is then manipulated in various ways to generate a realistic cirrus cloud.

In section 2 we show how cloud radar data are analysed to extract the parameters describing the 3D structure of cirrus. In section 3 the formulation of the model is outlined. Then in section 4, radiation calculations are performed to demonstrate the sensitivity of the fluxes to fallstreak orientation, which is determined by wind shear.

2 ANALYSIS OF CLOUD RADAR DATA

We use data recorded by the vertically pointing 94-GHz *Galileo* radar located at Chilbolton in Southern England. The approach is initially similar to Hogan and Illingworth (2003); radar reflectivity factor is converted to ice water content (IWC) using a power-law expression derived from aircraft data. Figure 1 shows a 2-hour time-height cross section of IWC through a cirrus cloud with a pronounced fall streak structure.

2.1 Probability density function

Hogan and Illingworth (2003) showed that the PDF of IWC tended to be well represented by a lognormal dis-

*Corresponding author address: Robin J. Hogan, Department of Meteorology, University of Reading, Earley Gate, PO Box 243, Reading RG6 6BB, UK; E-mail: r.j.hogan@reading.ac.uk.

†Current affiliation: Institute for Atmospheric and Climate Science, ETH, Zürich, Switzerland.

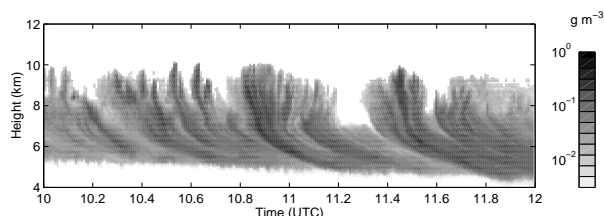


Figure 1: Ice water content derived from 94-GHz radar reflectivity on 26 December 1999.

tribution, and characterised the horizontal variability in terms of the fractional variance of IWC, f_{IWC} , which may be regarded as the variance of $\ln(IWC)$. We therefore constrain the stochastic model to produce lognormal IWC distributions with mean and fractional variance at each height derived from the radar data. Where there are gaps in the radar data due to reflectivities below the instrument sensitivity threshold, the data are analysed in such a way as to obtain the parameters of an “underlying” lognormal distribution which best fits the observed PDF in the upper part of its range.

2.2 Vertical structure

A striking feature of radar images of ice clouds is the fallstreak structure, whereby horizontal inhomogeneities caused by convective overturning at cloud top (the “generating level”) are carried down with the falling ice, but displaced horizontally with respect to cloud top due to the presence of vertical wind shear. Marshall (1953) showed that consideration of the profile of horizontal wind and mean particle fallspeed cloud be used to predict cirrus fallstreak geometry, and that constant vertical wind shear and constant fallspeed led to parabolic fallstreaks. We use essentially the same formulation as Marshall (1953), with the wind profile taken from the Met Office forecast model and a prescribed fallspeed. In principle the velocity measured by a Doppler radar could be used for fallspeed.

2.3 Horizontal structure

The radar data are first transformed from time to horizontal distance using the wind at cloud top, which in the case shown was 55 m s^{-1} . The horizontal structure is then characterised by taking power spectra of $\ln(IWC)$ at each height. Gaps in the radar data are replaced by a constant value below the radar sensitivity threshold. This does not significantly affect the resulting spectra, provided that the gaps do not constitute more than about 25% of the field.

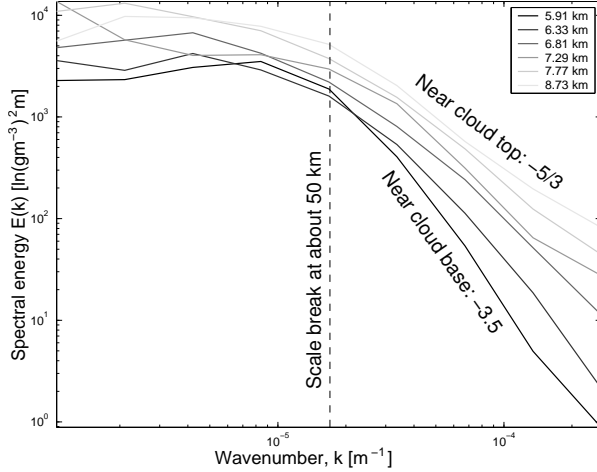


Figure 2: Power spectra of $\ln(\text{IWC})$ as a function of height for the data shown in Fig. 1. The raw spectra have been averaged such that there are around four points per decade of wavenumber.

The results for the cloud in Fig. 1 are shown in Fig. 2. It can be seen that near cloud top a spectral slope of $-5/3$ is evident. This indicates that here IWC is acting as a tracer of a turbulent field, presumably originating from convective overturning in the generating region. The fact that this behaviour is seen up to scales of 50–100 km indicates a 2D upscale cascade of energy (e.g. Lilly 1983) rather than 3D turbulence in the inertial subrange, although interaction with gravity waves could play a part. The reason for a scale break at 50–100 km is not certain, although it was clearly also evident in the f_{IWC} results of Hogan and Illingworth (2003), obtained from 18-months of data. Below cloud top there is a distinct steepening of the power spectra, indicating the suppression of structure preferentially at small scales. An explanation for this is variable particle fall speeds in the presence of vertical wind shear leading to different horizontal displacements (as predicted by the Marshall 1953 model) and hence a horizontal homogenisation.

The parameters of the spectrum provided to the stochastic model are simply the slope of the power spectrum at each height and the position of the scale break (which is assumed constant with height). At scales larger than the scale break, the power is taken to be constant with wavenumber. It should be noted that the absolute value of spectral energy does not need to be recorded, as this is implicitly provided by f_{IWC} which, by Parseval's Theorem, is simply the area under the power spectrum.

3 FORMULATION OF STOCHASTIC CLOUD MODEL

3.1 Generation of an isotropic fractal field

The first step is to generate a 3D isotropic field with a Gaussian PDF and a spectral slope of our choosing. Suppose that we wish the 1D power spectrum $E_1(k)$ through this field to have a single slope μ at all scales:

$$E_1(k) = \hat{E}_1 k^\mu, \quad (1)$$

where k is wavenumber and \hat{E}_1 is the spectral energy density at $k = 1 \text{ m}^{-1}$. Now, for the 3D field we are to generate there exists a 3D spectral energy density matrix $E_3(k_x, k_y, k_z)$, which is found by taking the 3D Fourier Transform of the field and multiplying each Fourier component by its complex conjugate (i.e. taking the square of the amplitude and discarding the phase information). Our approach is to reverse this process: if we can generate E_3 somehow then by assuming random phases for each of the Fourier components, a 3D inverse Fourier Transform will yield the required fractal field. A different set of random phases will produce a different realisation of the cloud field, but with the same statistical properties. For our field to be isotropic, E_3 must be a function of absolute wavenumber $k = (k_x^2 + k_y^2 + k_z^2)^{1/2}$ only. A 1D power spectrum through the field in the x -direction will satisfy

$$E_1(k_x) = \int_{-\infty}^{\infty} \int_{-\infty}^{\infty} E_3(k_x, k_y, k_z) dk_y dk_z. \quad (2)$$

With the constraint that the field is isotropic and that there is a single spectral slope, it can be shown that

$$E_3(k) = \hat{E}_3 k^{\mu-2}, \quad (3)$$

i.e. the 3D power spectrum is a simple power law and is steeper than E_1 by two powers of k . If there is a scale break in the 1D spectrum then this may be included at the same place in the 3D spectrum, but ensuring that the spectrum to each side of the break is still steeper than E_1 by k^2 . It should be noted that the value of \hat{E}_3 is arbitrary as the variance of the field will be later scaled by f_{IWC} .

The procedure described here is only really valid for cubic domains with the same grid spacing in the horizontal and vertical, whereas for cirrus we typically require a domain of around $L_x = L_y = 200 \text{ km}$ in the horizontal but only $L_z = 5 \text{ km}$ in the vertical, and similarly a vertical resolution of around $\Delta z = 100 \text{ m}$ compared with only $\Delta x = \Delta y = 1 \text{ km}$ in the horizontal. When (2) is reduced to a discrete summation this necessitates the introduction of two additional artificial scale breaks in E_3 (at Δx and L_z), in order that the 3D field has the required spectral properties. The details are unfortunately too involved to describe here.

3.2 Conversion to a realistic cloud field

The resulting 3D fractal field is then manipulated in various ways to simulate a realistic cirrus cloud. The first two steps, horizontal displacement (to simulate fall-streaks) and adjustment of the slope of the power spectrum (to simulate shear-induced mixing) are performed in the wavenumber domain. At each height a 2D Fourier Transform is performed. To simulate a horizontal translation of $(\delta x, \delta y)$, the Fourier coefficients are multiplied by $\exp(i\theta)$ where $\theta = 2\pi(k_x \delta x + k_y \delta y)$. To change the slope of the power spectrum from μ_1 to μ_2 , the Fourier components are then multiplied by $k^{(\mu_2 - \mu_1)/2}$, where k is the absolute wavenumber in 2D space. An inverse 2D Fourier Transform is then performed to recover the modified field.

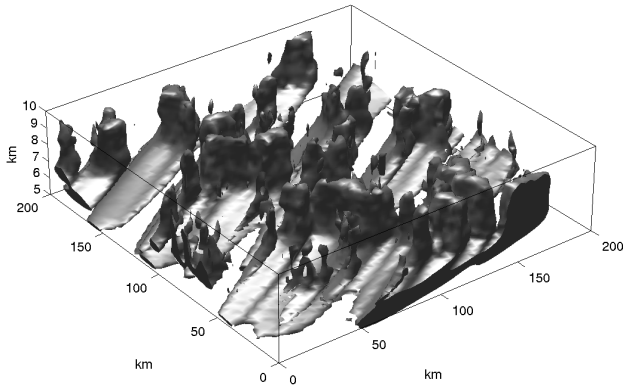


Figure 3: 3D visualisation of the 0.2 g m^{-3} IWC isosurface, for a simulation of the 26 December 1999 case.

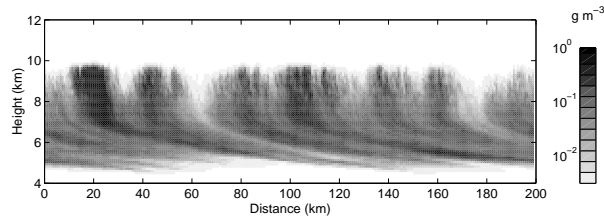


Figure 4: Cross-section of IWC through a simulation of the 26 December 1999 case; to be compared with Fig. 1.

At this stage the field has an approximately Gaussian distribution with a mean of zero and an arbitrary variance. The final step is to scale and threshold it. We scale each 2D slice of the field in order that that it has the variance f_{IWC} obtained from observations, then exponentiate it to yield a lognormal distribution. The resulting field is scaled again to obtain the required profile of mean IWC with height, and finally values below a certain threshold may be rejected to represent gaps in the cloud.

3.3 Example simulation

The model has been applied to the 26 December 1999 case discussed in section 2, and Figure 3 shows a 3D visualisation of the result. The fallstreak structures characteristic of cirrus are clearly evident, and a cross-section through the domain in Fig. 4 exhibits encouraging similarity to the original radar image in Fig. 1. Power spectra through the simulated cloud field are very similar to those in Fig. 2. It is evident in Fig. 3 that near cloud top the field is horizontally isotropic, while in real cirrus, gravity waves and shear can lead to roll-like structures in this region. While the model does not currently represent these anisotropic effects, the results of Hinkelman (2003) suggest that manipulation of E_3 could enable them to be simulated.

4 RADIATIVE PROPERTIES OF INHOMOGENEOUS CIRRUS CLOUDS

We now demonstrate how the stochastic model may be used to investigate the effect of cloud inhomogeneity (specifically fallstreak orientation) on the radiative properties of cirrus. An optically thinner cloud from 17 July 1999

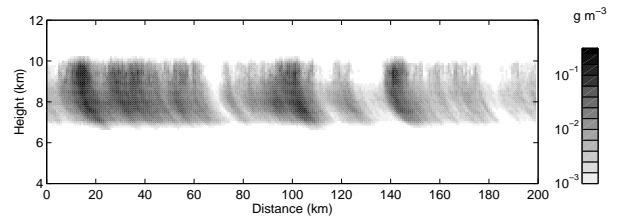


Figure 5: Cross-section of IWC through a simulated cirrus cloud based on observations from 17 July 1999, when the mean vertical shear through the cloud was $2 \text{ m s}^{-1} \text{ km}^{-1}$ (low shear case).

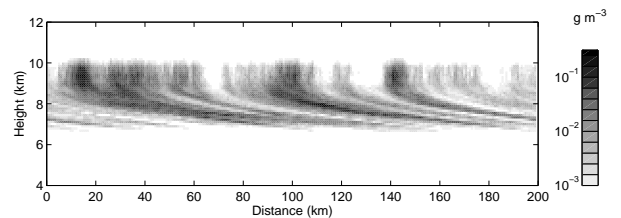


Figure 6: Cross-section through the same cloud as in Fig. 5, but with the wind velocity multiplied by 10 (high shear case).

is used, at which time the wind shear according to the Met Office model was low at around $2 \text{ m s}^{-1} \text{ km}^{-1}$. The simulation was performed on a domain measuring 200 km horizontally, with a resolution of 780 m in the horizontal and 50 m in the vertical. A cross-section through the domain is shown in Fig. 5. Figure 6 shows a second simulation performed with the same input parameters as the first (and with the random number generator seeded by the same value), except with the wind speed (and hence shear) a factor of 10 higher. This results in much more horizontally aligned fallstreaks, similar to those in Figs. 1 and 4. It should be stressed that the two fields have the same mean IWC at each height, and hence the same mean optical depth.

The effects of these fields on radiative fluxes are best illustrated by consideration of the shortwave albedo and longwave emissivity. Assuming a constant effective radius of $50 \mu\text{m}$ the vertically integrated IWC may be converted to shortwave optical depth, and assuming no horizontal transport of photons, to albedo. Figure 7 shows the albedo of the low and high shear cases, assuming a solar zenith angle of 60° and a surface albedo of 0.2, calculated using the Edwards-Slingo radiation code. These images are similar to what would be seen by a visible satellite imager. The fallstreaks are clearly visible in the second panel, and importantly there is an increase in the mean albedo of the field of 0.04, corresponding to an increase in reflected shortwave flux of around 25 W m^{-2} at this solar zenith angle. This represents a 20% increase in the top-of-atmosphere shortwave effect of the cloud.

Assuming the longwave extinction coefficient to be half the visible extinction coefficient, the corresponding emissivity of the cloud may be estimated, and is shown in Fig. 8. While emissivity is a rather crude parameter for describing the longwave properties of a cloud 3 km deep, it clearly illustrates how the horizontal alignment

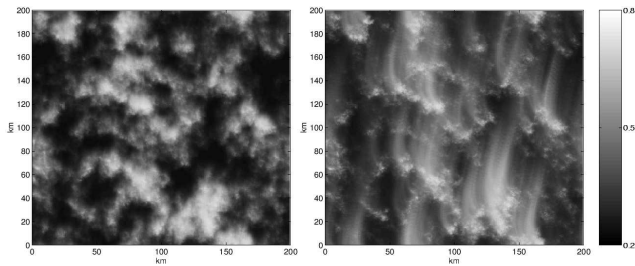


Figure 7: Albedo of simulated cloud in the low (left) and high (right) shear cases, the domain-mean albedos being 0.37 and 0.41 respectively.

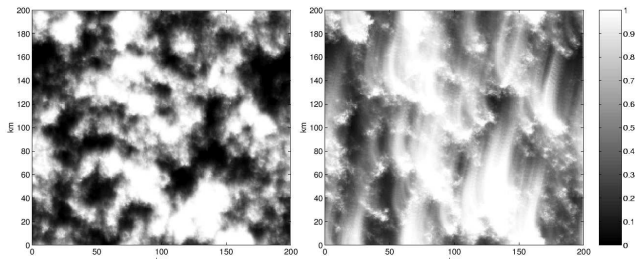


Figure 8: Emissivity of simulated cloud in the low (left) and high (right) shear cases, the domain-mean emissivities being 0.52 and 0.66 respectively.

of fallstreaks in high wind shear conditions leads to a greater fraction of the domain covered by “near black-body” clouds. For a mean cloud temperature of -50°C and a surface temperature of 10°C , the increase of mean emissivity from 0.52 to 0.66 corresponds to a reduction in outgoing longwave radiation of around 30 W m^{-2} , i.e. 30% of the top-of-atmosphere longwave effect of the cloud.

The reason for the effect on mean fluxes is that the relationships between optical depth and both albedo and emissivity are not linear, so even though the mean optical depth stays constant, the mean albedo and mean emissivity will change as the PDF of optical depth changes. The main curvature in the relationships occurs at lower optical depths in the case of emissivity, so longwave fluxes will tend to be more sensitive to the inhomogeneities of optically thin clouds than shortwave fluxes, with the converse being the case for optically thick clouds.

5 CONCLUSIONS

In this paper a stochastic model has been described for generating realistic 3D cirrus cloud fields from radar-derived power spectra. Simple radiative transfer calculations using the independent column approximation have demonstrated the strong effect of fallstreak geometry (which is in turn governed by wind shear) on both shortwave and longwave fluxes, highlighting the importance of cirrus inhomogeneity for climate and the need to represent it adequately in large-scale models. It should be noted that, by contrast, in the study of the effects of stratocumulus inhomogeneity, longwave fluxes are of little interest because the temperature contrast with the ground is much less, and because the higher optical

depth means that most of the cloud field behaves as a black body.

Future analysis will address some of the simplifications made here in estimating cloud radiative properties. The assumption of constant effective radius may be relaxed in two ways, either by applying the method of Evans and Wiscombe (2004) to generate an effective radius field simultaneously with IWC (with a specified correlation between the two), or by directly simulating extinction coefficient rather than IWC, as extinction is much more directly related to the radiative properties of the cloud in both the shortwave and longwave. Three-dimensional radiative transfer calculations will also be performed.

Another use for the model is in testing the performance of satellite retrieval algorithms, particularly those which involve the synergy of multiple instruments where coincident sampling of the cloud is important (such as spaceborne radar and lidar).

ACKNOWLEDGEMENTS

We are grateful to the Rutherford Appleton Laboratory for the use of the Galileo radar, to Malcolm Brooks for assistance in running the radiation code and to the Met Office for the model data. SFK was supported by a NERC studentship.

REFERENCES

- Cahalan, R. F., W. Ridgeway, W. J. Wiscombe, T. L. Bell and J. B. Snider, 1994: The albedo of fractal stratocumulus clouds. *J. Atmos. Sci.*, **51**, 2434–2455.
- Carlin, B., Q. Fu, U. Lohmann, G. G. Mace, K. Sassen and J. M. Comstock, 2002: High-cloud horizontal inhomogeneity and solar albedo bias. *J. Climate*, **15**, 2321–2339.
- DiGuseppe, F., and A. M. Tompkins, 2003: Effect of spatial organisation on solar radiative transfer in three dimensional idealized stratocumulus cloud fields. *J. Atmos. Sci.*, **60**, 1774–1794.
- Evans, K. F., and W. J. Wiscombe, 2004: An algorithm for generating stochastic cloud fields. *Submitted to Atmos. Res.*
- Hinkelman, L. M., 2003: *The effect of cumulus cloud field anisotropy on solar radiative fluxes and atmospheric heating rates*. PhD Thesis, The Pennsylvania State University.
- Hogan, R. J., and A. J. Illingworth, 2003: Parameterizing ice cloud inhomogeneity and the overlap of inhomogeneities using cloud radar data. *J. Atmos. Sci.*, **60**, 756–767.
- Lilly, D. K., 1983: Stratified turbulence and the mesoscale variability of the atmosphere. *J. Atmos. Sci.*, **40**, 749–761.
- Liou, K.-N., 1986: Influence of cirrus clouds on weather and climate processes: A global perspective. *Monthly Weather Rev.*, **114**, 1167–1199.
- Marshall, J. S., 1953: Precipitation trajectories and patterns. *J. Meteorol.*, **10**, 25–30.
- Pomroy, H. R., and A. J. Illingworth, 2000: Ice cloud inhomogeneity: Quantifying bias in emissivity from radar observations. *Geophys. Res. Lett.*, **27**, 2101–2104.